Thorough Investigation of the Oslo Model

Stefano Veroni

21st February 2022

Abstract: The Oslo model, is one of the simplest yet rich examples of a system displaying self-organised criticality. In this report, by analysing a Python simulation spanning 3 orders of magnitude, many features of the 1D Oslo model were qualitatively and quantitatively examined. It is shown that in the critical state the average slope $\langle z \rangle$ tends to a constant $a_0 = 1.734 \pm 0.006$, implying the average height scales linearly with size for $L \gg 1$. Furthermore, it is shown the steady state height distribution follows a skewed gaussian distribution, with skewness $\gamma_1 = 0.27$. It is proven the critical time scales quadratically with size. Finally, the avalanche exponents were determined $D = 2.24 \pm 0.03$ and $\tau_s = 1.56 \pm 0.03$. The avalanches in the bulk-driven height and charge models were also analysed, yielding $D = 1.24 \pm 0.03$, $\tau_s = 1.20 \pm 0.02$ and $D = 2.23 \pm 0.03$, $\tau_s = 1.12 \pm 0.04$.

Word count: 3479 words in the report. **2453** effective, as 1026 words are excluded from the count: 165 from the front page, 658 from figures and tables, 203 from Bibliography.

I. Introduction

The study of self-organised criticality (SOC), a concept first proposed in 1987 [1], has since then been extremely stimulating, finding multiple applications, from statistical mechanics to astrophysics, from materials science to neuroscience to sociology, and more[2].

The Oslo model, which describes the dynamics of a slowly driven pile of rice [3,4], is a simple yet non-trivial model displaying all key SOC features. The aim of this report is to investigate such features, by producing and analysing a python-based simulation spanning 3 orders of magnitudes in size.

II. Theory

Systems displaying SOC properties are composed of multiple units interacting with their neighbours and storing some charge intermediately with a local threshold. As slowly driven, they eventually reach a steady critical state with equal average influx and outflux[5].

These conditions lead to intermittent relaxation events spanning a broad range of orders of magnitude with no typical size. Their frequency usually follows a power-law decay, with some cutoff size dictated by the size of the system[5].

For the 1D Oslo "ricepile" model, consider a lattice composed of L sites $i = 1, 2, \dots, L$, as in Fig 2.1. The height h_i of each site is defined as the number of grains it contains, while the slope z_i is the difference in the height of neighbouring sites, as

$$z_i = h_i - h_{i+1}, \tag{2.1}$$

where h_{L+1} is set to zero. h_1 is defined as the height of the pile.

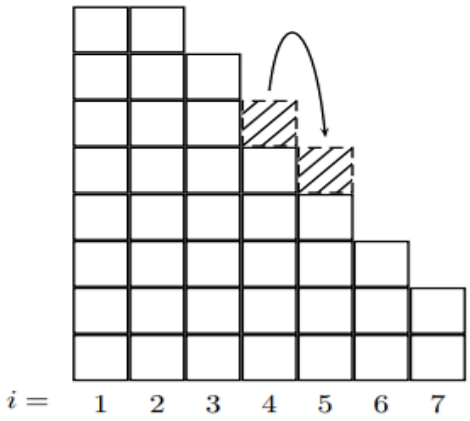

Figure 2.1 An Oslo model ricepile, with site 4 toppling. Adapted from [6].

Each site has a threshold $z_i^{th} \in \{1,2\}$ randomly assigned with probabilities $\{p, 1-p\}$, such that, if $z_i > z_i^{th}$, the site topples and one grain falls onto the next site. The pile is boundary-driven by adding one grain at site $i = 1$ and allowing for relaxation, i.e. for all sites to topple until a stable configuration is reached.

When the i^{th} site topples, z_i^{th} is assigned again. The full relaxation event induced by an added grain is defined as avalanche, with its size s being the number of topplings.

After a grain leaves the pile, i.e. the L^{th} site topples, the pile enters in the critical state, with

$$\langle \text{influx} \rangle = \langle \text{outflux} \rangle, \tag{2.2}$$

and displays SOC features. The critical time t_c is defined as the number of grains added to an empty pile before the first leaves the system.

After the pile is initialised in a stable configuration, its dynamics can be described algorithmically in terms of $\{z_i\}$, with following steps:

1. Drive. Add a grain at site $i = 1$, such that
$$z_1 \to z_i + 1. \tag{2.3}$$
2. Relaxation. As $z_i > z_i^{th}$, relax the site, with some different mechanisms at the boundaries.
For $i = 1$:
$$\begin{matrix} z_1 \to z_1 - 2 \\ z_2 \to z_2 + 1 \end{matrix}. \tag{2.4a}$$
For $i = 2, 3, \dots, L-1$:
$$\begin{matrix} z_i \to z_i - 2 \\ z_{i\pm1} \to z_{i\pm1} + 1 \end{matrix}. \tag{2.4b}$$
For $i = L$:
$$\begin{matrix} z_{L-1} \to z_{L-1} + 1 \\ z_L \to z_L - 1 \end{matrix}. \tag{2.4c}$$
Once a site has toppled, a new threshold is assigned to it, at random, as
$$z_i^{th} = \begin{cases} 1 & \text{with probability } p \\ 2 & \text{with probability } 1-p \end{cases}. \tag{2.5}$$
Repeat for all sites, until $z_i < z_i^{th}\ \forall i$.
3. Iterate. Repeat from step (1).

p was set to $1/2$, unless were explicitly stated, thus leading to z^{th} being assigned as 1 or 2 with equal probability.

III. Testing

Before carrying out the actual investigations, the correctness of the python code was verified by a set of tests.

A. Height of the Pile

The height of the ricepile in the critical state for lattice sizes 16 and 32 was known to be approximately 26.5 and 53.9 respectively[7].

Ricepiles of such sizes were driven with a million grains each to record an accurate estimate of the time-averaged height $\langle h \rangle$. The procedure was repeated 10 times, to obtain an average $\widetilde{\langle h \rangle}$ of such averages $\langle h \rangle_j$, with corresponding standard deviation $\sigma_{\widetilde{\langle h \rangle}}$.

The results were $\widetilde{\langle h \rangle} = 26.530 \pm 0.003$ and 53.887 ± 0.003, in both cases extremely close to the known approximate values, as required.

B. Boundary-Driven BTW Sandpile

When p in Eq. 2.5 is set to 1, the maximum threshold is fixed as 1 at all sites. The ricepile should then exhibit the properties of a boundary driven BTW "sandpile" [1,5] .

This implies its critical time must be $t_c = L(L+1)/2$, and, in the critical state, $z_i = 1\ \forall i$, hence fixing the critical height of the pile to L, and $s = L$ for all avalanches.

The model was tested for $L = 16, 32, 64, 128$, for 100,000 grains each, yielding the expected results.

C. Recurrent Configurations

The number of possible recurrent configurations of the pile is[5]

$$N_{\mathcal{R}} = \frac{1}{\sqrt{5}}\left[\phi(\phi+1)^L + \frac{1}{\phi(\phi+1)^L}\right] \approx \frac{\phi}{\sqrt{5}}(1+\phi)^L \quad for\ L \gg 1, \qquad (3.1)$$

where ϕ is the golden number. The test consisted in tracking the number of different recurrent configurations the system exhibits while driven in critical state to compare it to the theoretical prediction. As $N_{\mathcal{R}}$ grows exponentially, the test was performed for small L only.

As the most extreme configurations, i.e. those close to the minimum configuration $z_i = 1\ \forall i$ and the maximum $z_i = 2\ \forall i$, are much less probable than the others, the test was devised to first set the pile in the minimum recurrent configuration and add 10,000 grains, then in the maximum, and add other 10,000 grains. This was repeated for $N = 2000$ times. The results are shown in Table 3.1

Table 3.1: Observation of Recurrent Configurations

The table shows, for each L, the number of different recurrent configurations found after n iterations, where each iteration involves 10,000 grains added starting from the minimum configuration, and 10,000 from the maximum.

L\Iterations	100	200	600	1000	1500	2000	$N_{\mathcal{R}}$
4	34	34	34	34	34	34	34
5	86	88	88	89	89	89	89
6	196	200	204	208	214	218	233
7	441	461	487	499	509	515	610
8	912	983	1072	1086	1121	1135	1539

As it can be observed, for very small L, i.e. 4 and 5, the number of recurrent configurations found exactly matches the theoretical expectations. For higher L, the number of recurrent configurations found increases with the number of iterations, as expected, although not able of finding them all. However, the important observation is that the testing results agree with the model.

IV. Height and Slope

Ricepiles with sizes $L \in \{4,8,16,32,\dots,1024\}$ were simulated. The total time T, measured in number of grains added to the system, was

$$T(L) = \max\left\{5 \times 10^6,\ \ 20 \times 10^6 \log_2\left(\frac{L}{1024}\right)\right\}, \tag{4.1}$$

to ensure a high statistic for all ricepiles. The time evolution of the ricepile's height is shown in Fig 4.1. It increases steadily, evolving through different transient configurations, until some time $t_c(L)$, when it starts to oscillate through recurrent configurations about a mean value $\langle h \rangle$.

The amplitude of the oscillations is relatively small, meaning that, as assumed in section III.C, recurrent configurations have unequal probability of being visited: those having height close to $\langle h \rangle$, the attractor of the dynamics, occur frequently, whereas the ones closer to the extrema are far less probable.

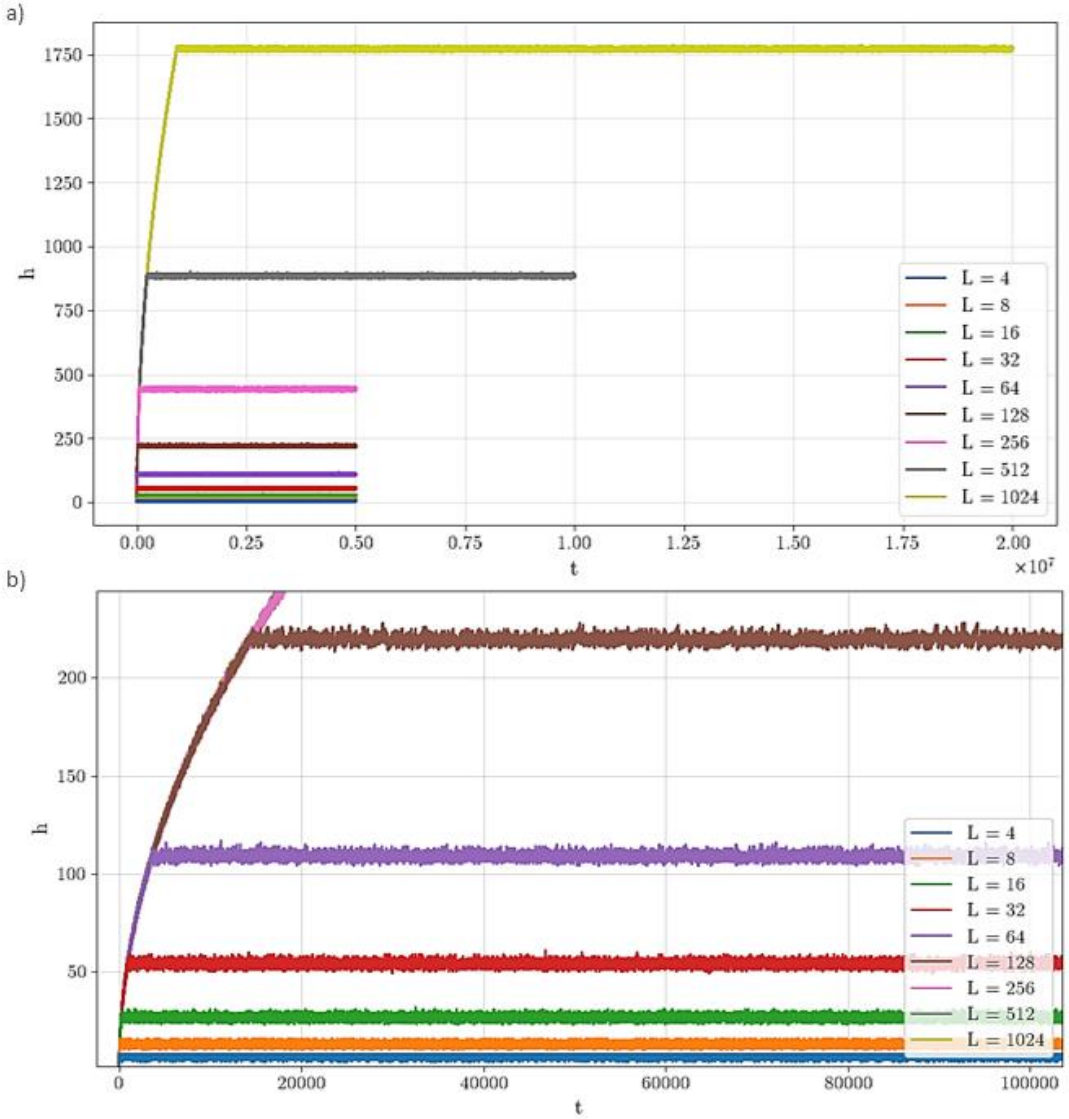

Figure 4.1. The time evolution of the height of the pile. (a) The height increases steadily until the attractor of the dynamics is reached, at which point it oscillates about some mean value. (b) Detail of the plot confirming small-L piles exhibit same behaviour and giving rough estimate of the amplitude of the oscillations in critical state.

A. *Mean Height and Slope*

The slopes z_i behave identically at all sites but the boundaries, hence the average slope $\langle z \rangle$ would be expected to be the same constant a_0 at all sites, with corrections for the boundaries. Therefore

$$\langle h \rangle = \sum_{i=1}^{L} \langle z_i \rangle \sim a_0 L. \tag{4.2}$$

The corrections should be negligible for $L \gg 1$, where the boundaries would represent a minimal portion of all sites, hence only affecting small-L piles. Mathematically, this implies

$$\langle h \rangle = a_0 L(1 - a_1 L^{-\omega 1}), \tag{4.3}$$

for some constants a_1 and ω_1, with $\omega_1 > 0$. Note that Eq. 4.3 is equivalent to

$$\log\left(1 - \frac{\langle h \rangle}{a_0 L}\right) = -\omega_1 \log L - \log a_1, \tag{4.4}$$

with the right hand side being the equation of a straight line in $\log L$. Thus, the best fit of a_0 is the one leading to the straightest left hand side. Eq. 4.3 and Eq 4.4 were separately fitted, and their results averaged, yielding: $a_0 = 1.734 \pm 0.006,\ a_1 = 0.24 \pm 0.17,\ \omega_1 = 0.62 \pm 0.20$. The statistical uncertainties on a_0 and ω_1 are relatively high mainly as they are "corrective constants", which are only valuable for small L. Our focus is the large-L behaviour, hence a further examination of such constants was beyond the scope of this investigation.

Fig. 4.2(a) and (b) show the results of the fit of Eq 4.3 and Eq 4.4 respectively. Note in Fig 4.2(b), the fit fails to satisfactorily include data for small L, implying the correction in Eq. 4.3 is not exact.

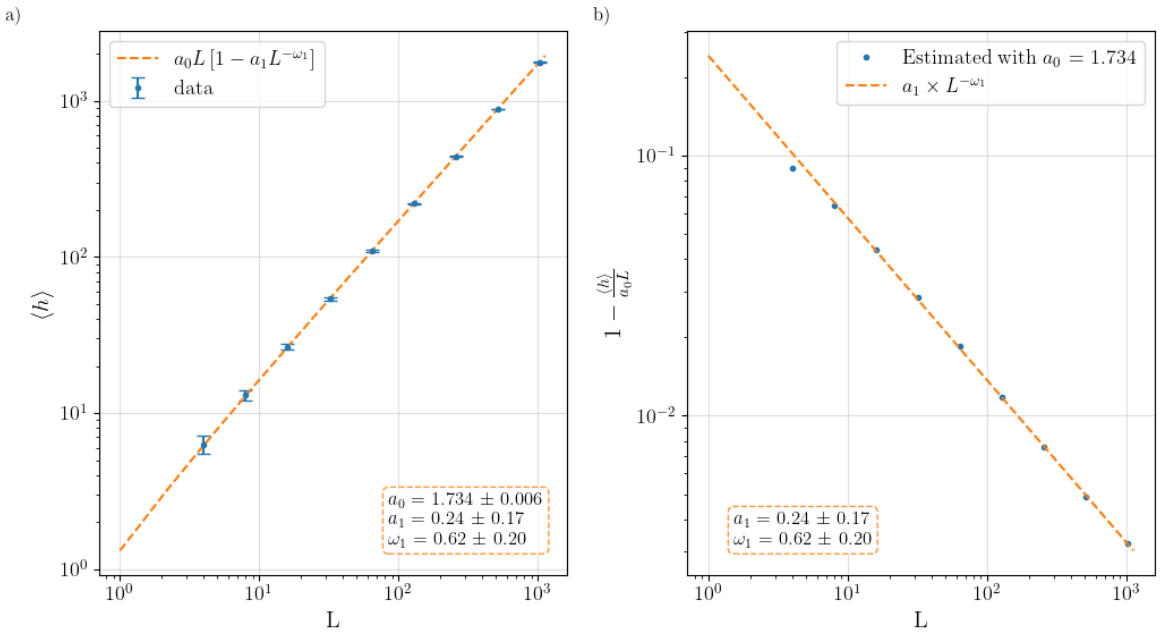

Figure 4.2 (a) Estimates $a_0 = 1.734, a_1 = 0.2, \omega_1 = 0.6$ show perfect agreement with Eq 4.3. (b) As suggested in Eq 4.4, the best a_0 fit leads to $1 - \langle h \rangle/(a_0 L)$ defining a straight line in logarithmic scale for $L \gg 1$, with small-L data departing from the fit.

The overall correctness of the model is confirmed by considering Fig 4.3, comparing a_0 with estimates of the slope of the pile $\langle z \rangle$, defined as

$$\langle z \rangle = \frac{1}{L}\sum_{i=1}^{L}\langle z_i \rangle = \frac{\langle h \rangle}{L}. \tag{4.5}$$

As expected, the mean slope tends to a_0, with the value being smaller for small L due to corrections at the boundaries. Note a_0 is bigger than the average z^{th}: this is because $z_i^{th} = 2$ is a more stable threshold, causing an upward shift in the slope of the stable configurations.

The standard deviation σ_h was then fitted resulting in a power law of form $\sigma_h = A\,L^{\chi}$, with $A = 0.579 \pm 0.002$ and $\chi = 0.241 \pm 0.001$, meaning it increases sub-linearly with L.From Eq. 4.5, the deviations on $\langle h \rangle$ and $\langle z \rangle$ can be deduced being related as

$$\sigma_z = \frac{d\langle z \rangle}{d\langle h \rangle}\sigma_h = \frac{\sigma_h}{L}. \tag{4.6}$$

implying $\sigma_z \to 0$ for $L \gg 1$, again confirming $\langle z \rangle$ tends to the constant a_0 more accurately with increasing L. The behaviour of the standard deviations is shown in Fig 4.4.

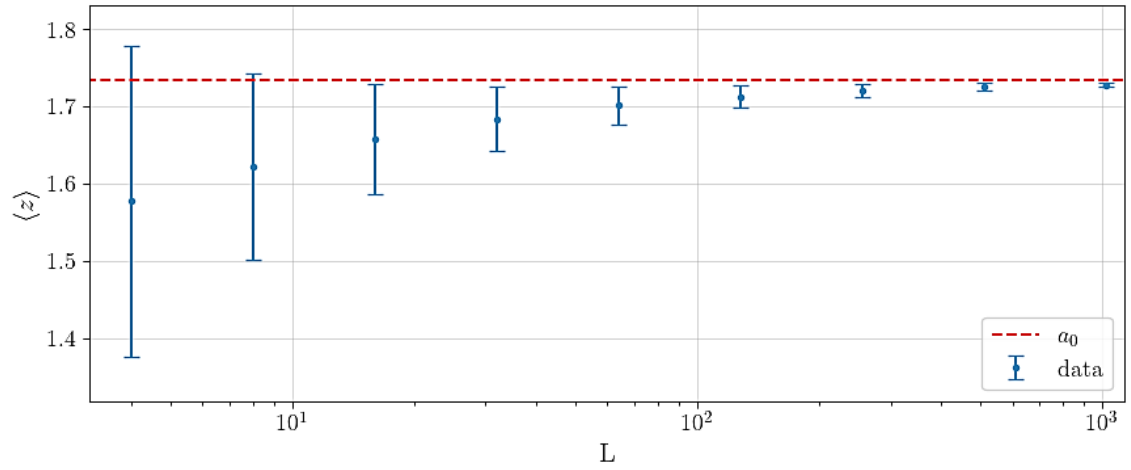

Figure 4.3 The average slope tends to $a_0 = 1.734$ with increasing L, while the deviation decreases.

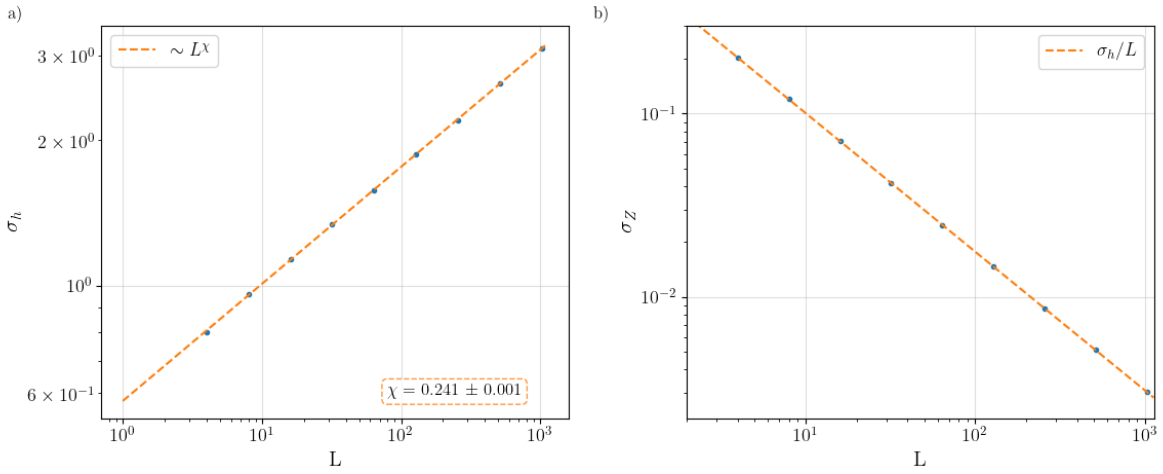

Figure 4.4. (a)The standard deviation of the height increases sub-linearly with L. (b) The standard deviation of the slope decreases tending to 0, confirming $\langle z \rangle$ tends to a constant with increasing L.

B. *Height Distribution*

Finally, let's consider the distribution of the heights in the critical state. Based on the assumption z_i are independent random variables, from central limit theorem, we would expect a gaussian distribution, with the independence of z_i suggesting σ_z should be independent of L. This would then imply

$$P(h;L) = \frac{1}{\sqrt{2\pi}\sigma_h} e^{-\frac{(h-\langle h\rangle)^2}{2\sigma_h^2}}, \tag{4.7}$$

with, based on Eq. 4.6, $\sigma_h \sim L$. However, results in section IV.A disprove such assumption. The height distributions are plotted in Fig 4.5.

Although $\sigma_h \nsim L$, a data collapse was implemented to assess Eq. 4.7. As, both $\langle h\rangle$ and σ_h are measured functions of L, we can rearrange Eq 4.7 as

$$\sigma_h P\left(\frac{h-\langle h\rangle}{\sigma_h}; L\right) = \frac{1}{\sqrt{2\pi}} e^{-\frac{1}{2}\left(\frac{h-\langle h\rangle}{\sigma_h}\right)^2} = G\left(\frac{h-\langle h\rangle}{\sigma_h}\right), \tag{4.8}$$

so that $G(x)$ resembles a normalised Gaussian centred in the origin for all L. The collapsed data is shown in Fig 4.6. As it can be observed, data from all ricepiles collapses nicely.

However, the distribution is positively skewed: the peak is slightly shifted to the left, and there is a longer tail to the right. This implies h is more likely to be much bigger than $\langle h\rangle$, rather than much smaller, and it was considered a consequence of the greater stability given by a greater z^{th}. The skewness of the collapsed distribution was assessed with Fisher-Pearson test[8]: the symmetric-gaussian model was rejected with p-value 0 (underflow) and the measured skewness was $\gamma_1 = 0.27$.

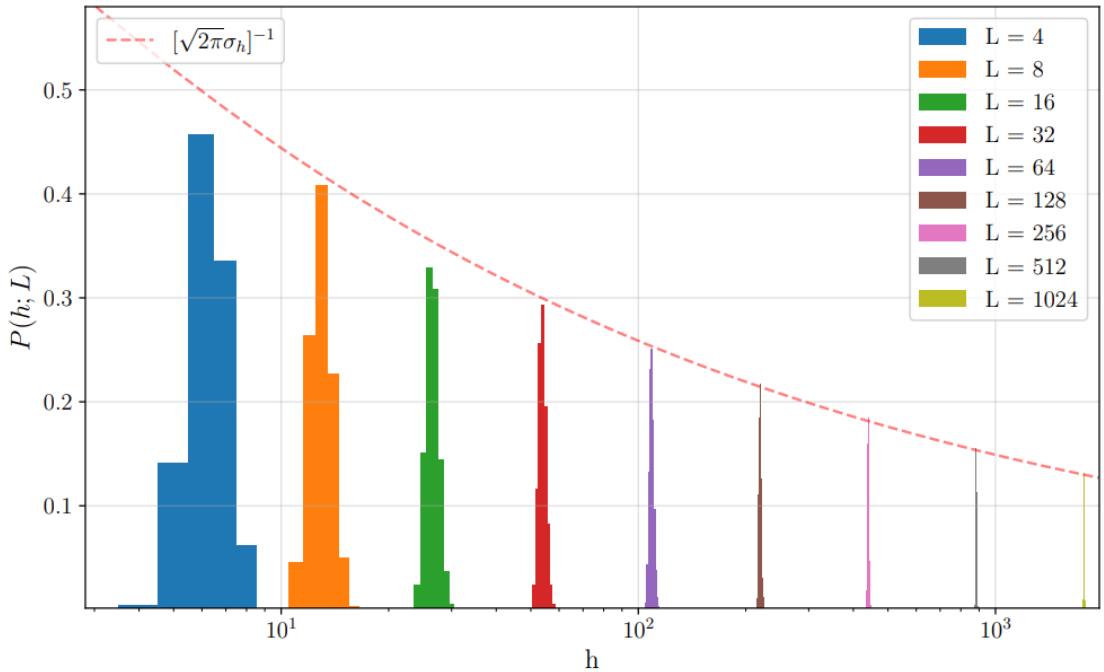

Figure 4.5 The height distributions are plotted with logarithmic x-scale, appearing to be well approximated by a gaussian for all L, with deviation, and consequently peaks' height too, scaling as expected, especially for L ≫ 1.

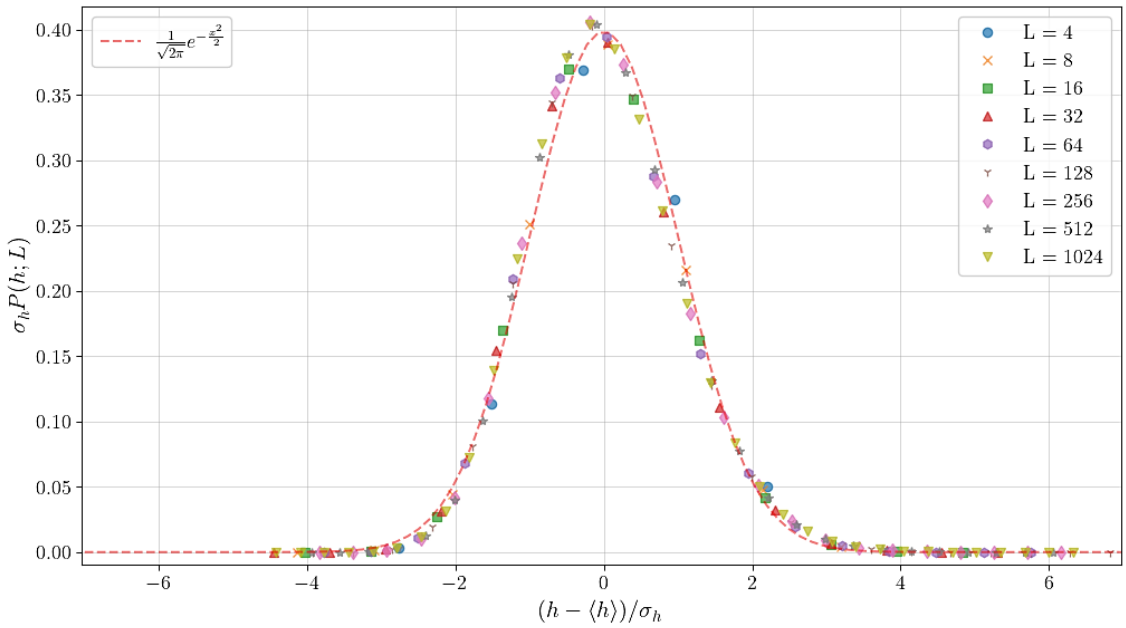

Figure 4.6. The data collapse further confirms P(h; L) has a gaussian-like shape, although positively skewed. The skewness was estimated as $\gamma_1 = 0.27$.

V. Time Evolution

As t_c is the number of grains added to the empty system immediately before it enters the critical state, it can be thought as the area of the pile. As $h_c \sim a_0 L$, we geometrically deduce

$$t_c \sim A_t L^2, \tag{5.1}$$

with $A_t \sim a_0/2$. To investigate this hypothesis, 30 realisations of ricepiles with sizes $L \in \{4,8,16,\dots,1024\}$ were simulated, each driven for $T = 3 \times L^2$. The height evolution and critical time were averaged, yielding $\tilde{h}(t;L)$ and $\widetilde{t_c}(L)$. Eq 5.1 was fitted, yielding $A_t = 0.859549 \pm 4 \times 10^{-6}$, and, as plotted in Fig 5.1, it shows perfect agreement with simulated data. A_t is slightly smaller than $a_0/2$ as corrections from Eq 4.3 were not implemented.

As time scales quadratically with size, whereas height does so approximately linearly, a data collapse for all L was suggested with shape

$$\frac{\tilde{h}}{L} \sim \mathcal{F}\left(\frac{t}{L^2}\right) \equiv \mathcal{F}(x). \tag{5.2a}$$

As $h_c \sim a_0 L$, past the critical time, i.e. for $x \geq A_t$, the scaling ansatz $\mathcal{F}(x)$ should tend to the constant a_0. For $t < t_c$, being t the number of grains in the system at that moment, we expect

$$t \sim \frac{1}{2}\tilde{h}(t) L_{eff}(t), \tag{5.3}$$

where $L_{eff}(t)$ is the effective size of the pile at time t, i.e. the index of the last non-empty site. At that moment, the pile effectively behaves as a pile of lattice size L_{eff}, hence $h(t) \sim a_0 L_{eff}(t)$. Then, substituting, and rearranging:

$$\tilde{h}(t) \sim \sqrt{2 a_0 t}, \tag{5.4}$$

which, dividing by L, yields

$$\frac{\tilde{h}(t)}{L} \sim \sqrt{2a_0 \frac{t}{L^2}} = \mathcal{F}\left(\frac{t}{L^2}\right) \quad for\ t < t_c\ . \tag{5.5}$$

Accordingly scaling the average height $\tilde{h}(t;L)$ and time, a data collapse was produced, as shown in Fig 5.2(a). Large-L data perfectly match the ansatz in Eq 5.3a, with small-L needing corrections. These were implemented, according to Eq. 4.3, leading to

$$\frac{\tilde{h}}{\langle h \rangle}(t;L) \sim \sqrt{2a_0 \frac{t}{L^2}}. \tag{5.2b}$$

As shown in Fig 5.2(b), it clearly improved the quality of the collapse, although still not quite matching the ansatz for $t < t_c$. Finally, note a_0 was here fitted as 1.72 ± 0.01, suggesting the relation in Eq 5.2b is not exact.

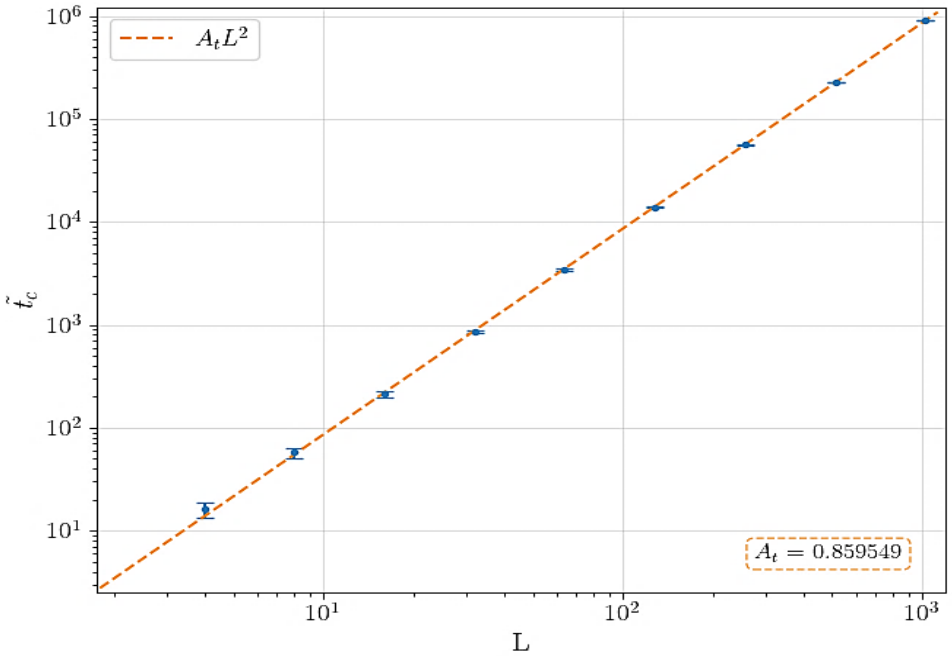

Figure 5.1. The average $\langle t_c(L) \rangle$ scales quadratically with lattice size L. The proportionality constant A_t well approximates $a_0/2$, although slightly smaller, as corrections for small L were not applied.

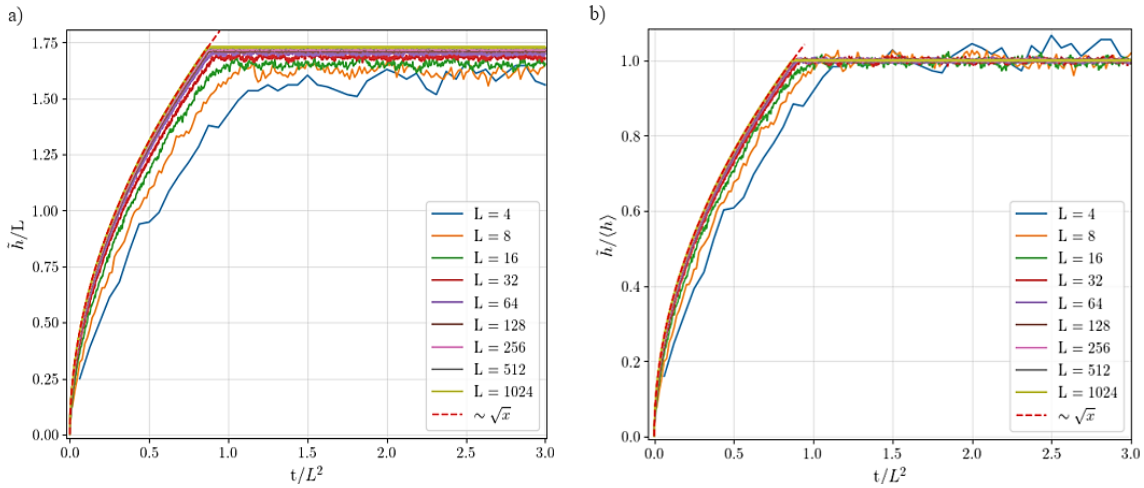

Figure 5.2. (a) The data collapse based on Eq 5.3a holds for $L \gtrsim 32$, but it poorly fits small L data. (b) Correction to the collapse based on Eq 4.3 improves its quality, especially for $t > t_c$, although a perfect matching was not obtained.

VI. Avalanches

The probability $P(s;L)$ of an avalanche in critical state having size s, derived from the same ricepiles used for section IV, is plotted in Fig 6.1. P(s; L) decreases following a power law $s^{-\tau_s}$, with τ_s being the same for all L, before falling steeply once a cutoff length s_c is met.

The fall is anticipated by a bump corresponding to avalanches reaching the boundary and causing grains to leave the system. These could be larger in a larger system, but, due to its finiteness, are reduced in size and accumulate as an excess in the tail of $P(s;L)$.

For $L \gg 1$, the cutoff is expected to scale as $s_c \sim L^D$ [5] and P(s; L) can be described by the ansatz [5]

$$P(s;L) = s^{-\tau_s}\mathcal{G}\left(\frac{s}{s_c}\right) = s^{-\tau_s}\mathcal{G}\left(\frac{s}{L^D}\right), \tag{6.1}$$

with $\mathcal{G}(x)$ rapidly decaying for $x > 1$.

A data collapse was used to investigate this hypothesis, aimed to matching the bumps' tops, with shape

$$s^{\tau_s}P\left(\frac{s}{L^D};L\right) = \mathcal{G}\left(\frac{s}{L^D}\right) = \mathcal{G}(x). \tag{6.2}$$

Results, shown in Fig 6.2, agree with literature values $D = 2.25$ and $\tau_s = 1.556$[5,6], apart for small L values.

Since both theory and results shown in Fig 6.2 suggest Eq. 6.1 to be valid for $L \gg 1$ only, any $L < 50$ was excluded from further investigation.

This was carried out by analysing the moments of avalanche sizes $\langle s^k \rangle$. In fact, the scaling ansatz in Eq 6.1 implies that [5]

$$\langle s^k \rangle \propto L^{D(k+1-\tau_s)} \text{ for } L \gg 1, \quad k \geq 1. \tag{6.3}$$

Eq 6.3 was rearranged as

$$\log\langle s^k \rangle = D(k+1-\tau_s)\log L + c, \tag{6.4}$$

as plotted in Fig 6.3 (a), and, by fitting, the slope $D(k+1-\tau_s)$ was inferred as a function of k, as shown in Fig 6.3 (b).

The fitted exponents estimates were $D = 2.24 \pm 0.03$ and $\tau_s = 1.56 \pm 0.03$. These agree with literature [5, 6] and with hypothesised $D = 9/4$ and $\tau_s = 14/9$, and imply $D(2-\tau_s) = 1$, hence confirming [5]

$$\langle s \rangle \propto L. \tag{6.5}$$

Collapse results are shown in Fig 6.4, showing perfect match for all L.

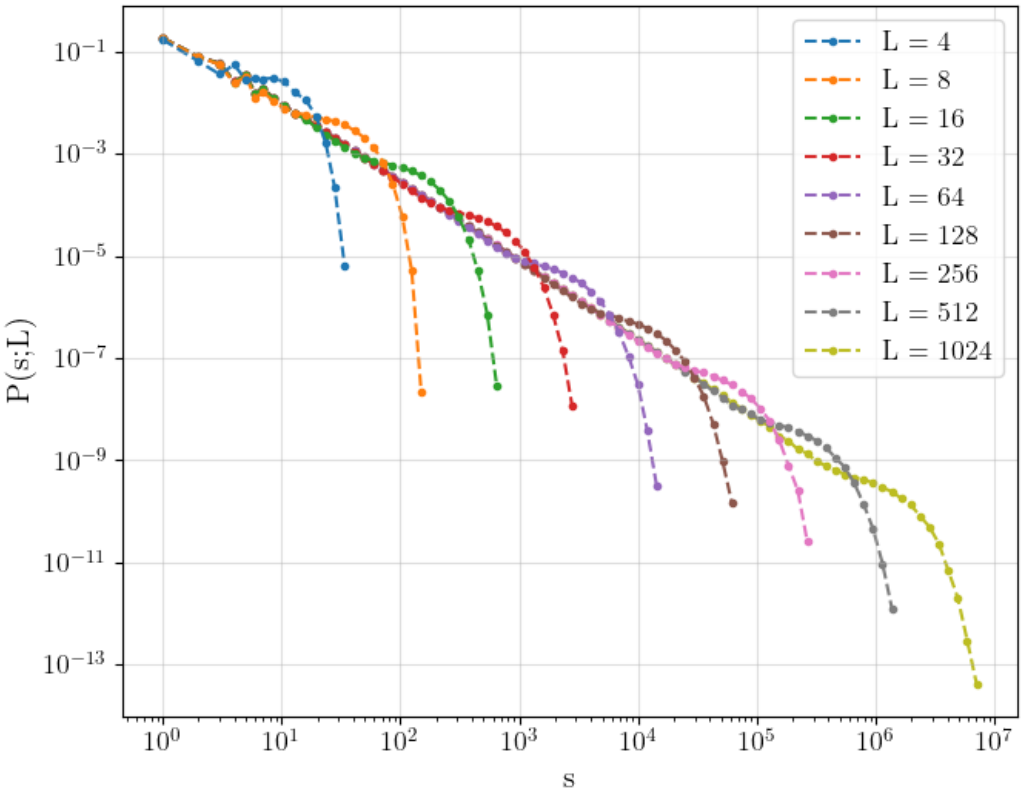

Figure 6.1 The avalanche-size probabilities scales with a negative power law, seemingly with same exponent τ_s for all L, until a cutoff size s_c is met. A log-binning method was used, with scaling factor 1.2, to ensure a high enough statistics in all bins.

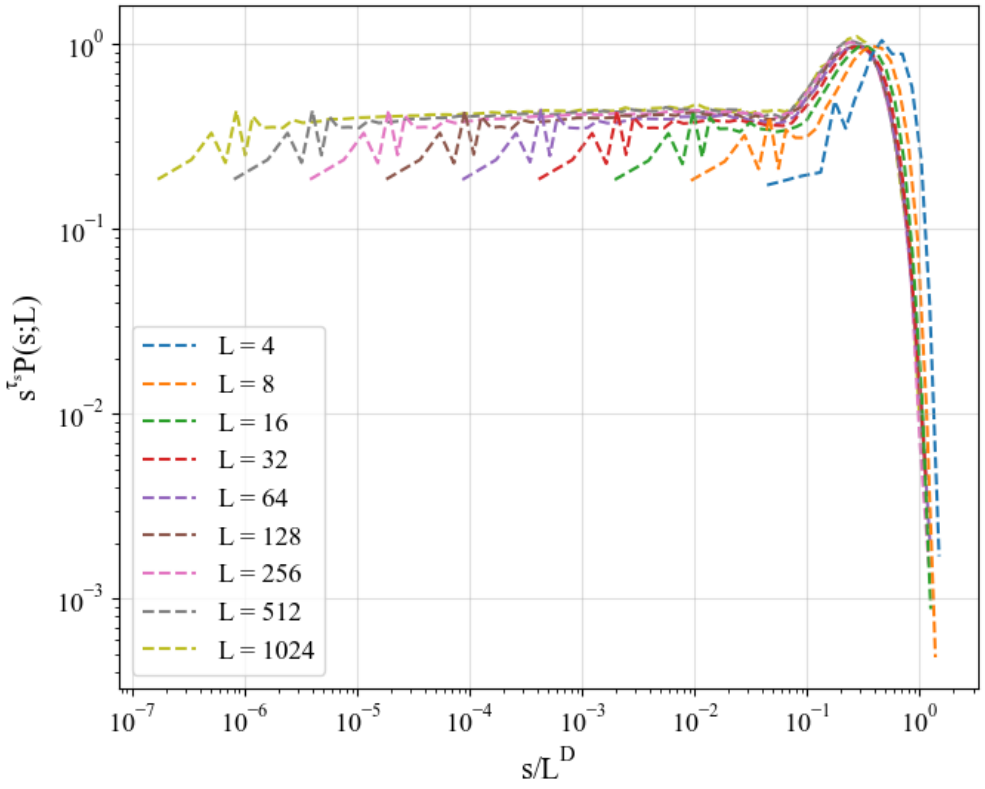

Figure 6.2 The data collapse with literature values $D = 2.25, \tau_s = 1.556$[5,6] agrees for L≫1. The zig-zag pattern for small s arises as a consequence of parity effects in L [9].

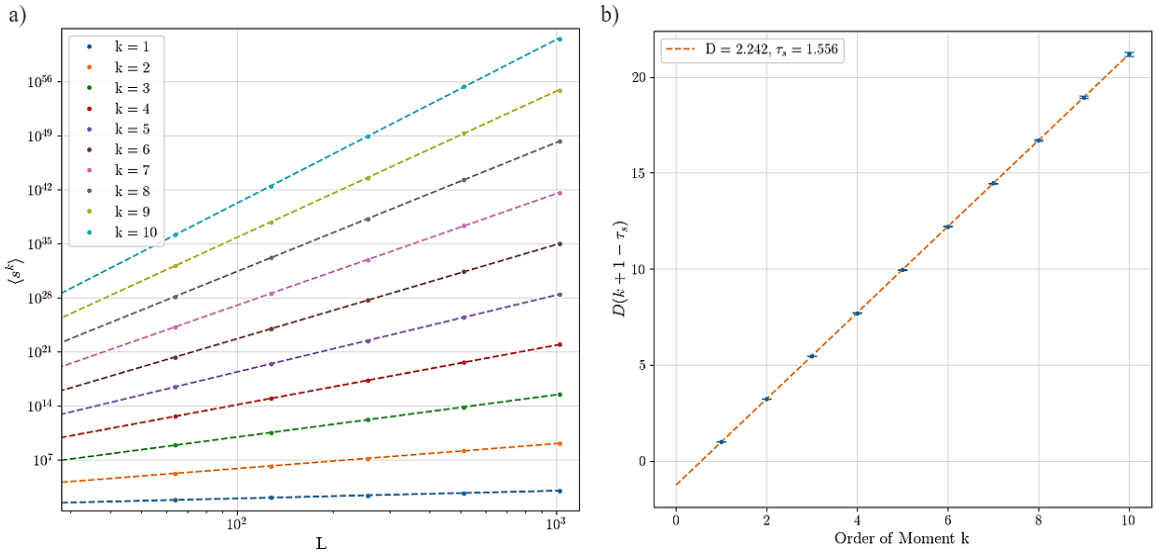

Figure 6.3 (a) The average k^{th} moment is plotted vs L for $k \in \{1,2,\ldots,10\}$, for large $L > 50$. (b) The coefficients $D(1 + k - \tau_s)$ which were obtained as the slopes of the lines in (a) lead to the estimation of $D = 2.242$ and $\tau_s = 1.556$, in perfect agreement with literature values [5,6].

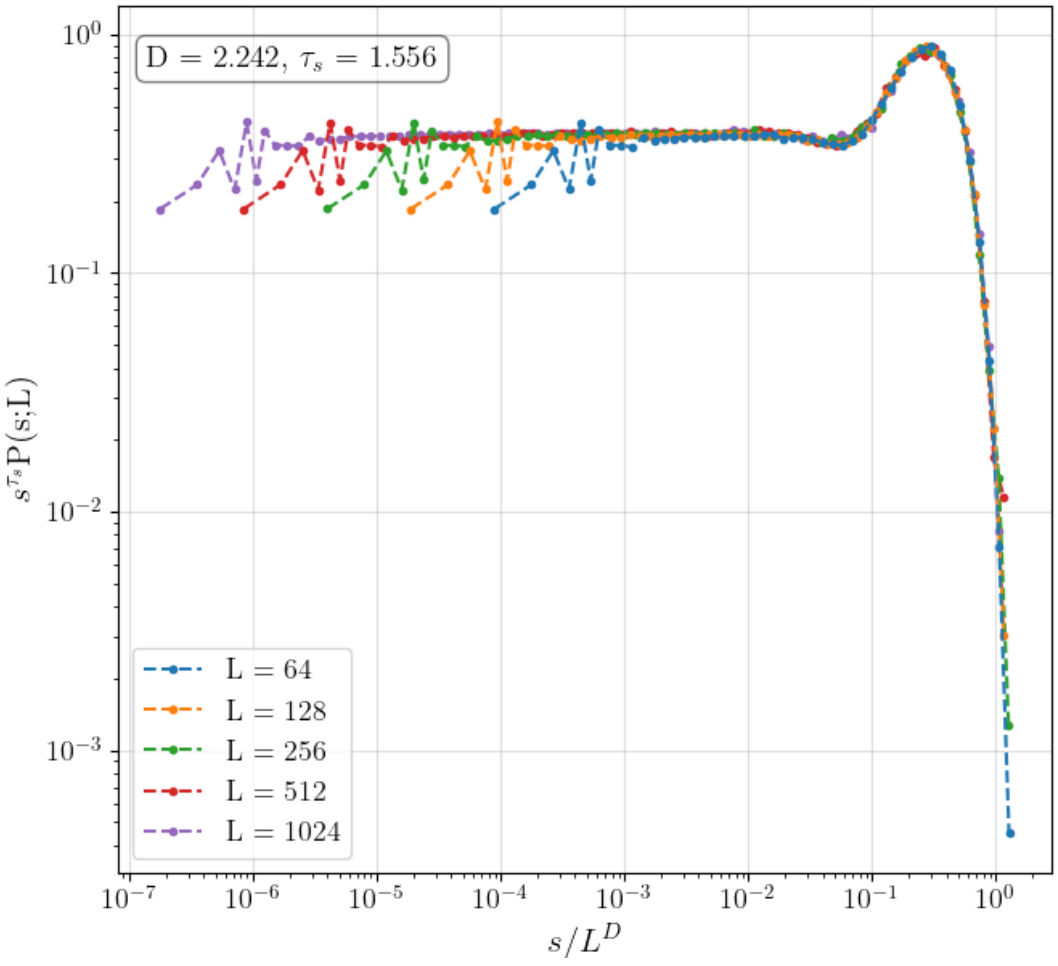

Figure 6.4 The collapse, with $L > 50$, shows perfect match.

VII. The Bulk-Driven Oslo Model

The model can be modified to be driven at any site at random. Two bulk-driven models can be formulated [6].

In the first, which I define bulk-height-driven (BHD) model, a physical block is added to a site i chosen at random, thus having driving equation

$$\begin{matrix} z_i \to z_i + 1 \\ z_{i-1} \to z_{i-1} - 1 \end{matrix}. \qquad (7.1a)$$

In the second, the bulk-slope-driven (BSD) model, a slope charge is added, hence

$$z_i \to z_i + 1. \qquad (7.1b)$$

This is physically less intuitive, ideally representing a pile in which one block is added to all j sites with $j \leq i$. However, it is more easily contextualised in the framework of SOC, in which the charge is the key quantity.

For both, due to increasing computational effort, piles of size up to 512 were simulated, with up to 5 million grains. Then, the procedure in section VI was applied. The estimated quantities, agreeing with literature [5,6,10], are shown in Table 7.1, while $\mathrm{P(s;L)}$ and collapse data are shown in Fig 7.1.

Table 7.1: Scaling Estimates

The table shows and compares the estimates on the quantities characterising the avalanches behaviour of the analysed models. Boundary driven and BHD models have similar $\langle s \rangle \propto L$ relation, but different exponents. Boundary driven and BSD models have different $\langle s \rangle$ behaviour, but matching D exponent.

Model	D	τ_s	$D(2-\tau_s)$	$\langle s \rangle$
Boundary Driven	2.24 ± 0.03	1.56 ± 0.03	~ 1	$\sim L$
Bulk Driven (Height)	1.24 ± 0.03	1.20 ± 0.02	~ 1	$\sim L$
Bulk Driven (Slope)	2.23 ± 0.03	1.12 ± 0.04	~ 2	$\sim L^2$

Boundary-driven and BHD models, both corresponding to a well-defined physical picture, agree on $D(2-\tau_s) = 1$, hence on the physical relation $\langle s \rangle \sim L$.

Oppositely, boundary-driven and BSD models appear to have very similar if not same D, which may thus be argued to be a more fundamental exponent in the context of the model.

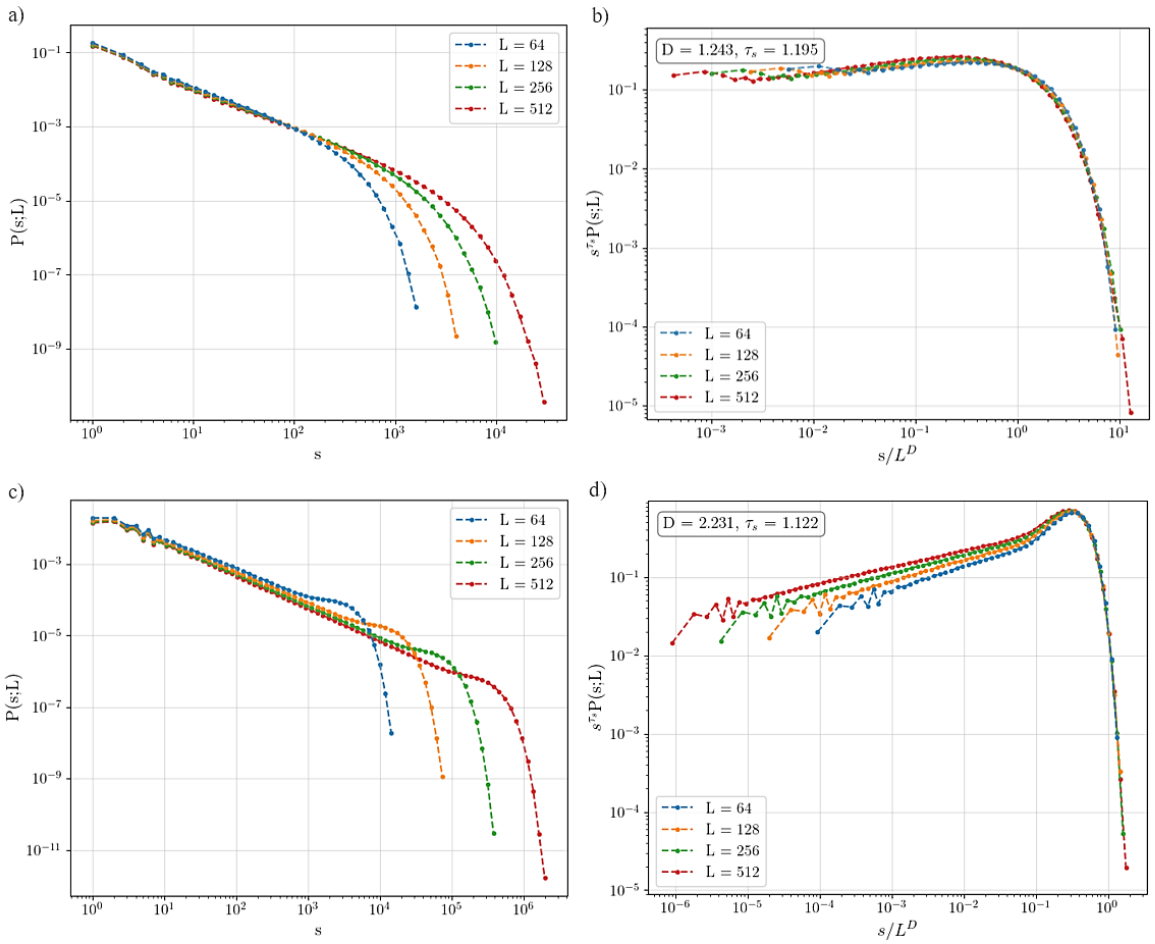

Figure 7.1 (a) P(s; L) for BHD model falls as power law, until a cut off length is reached. Note the maximum s is smaller than in the boundary-driven model. (b) The data collapse for the BDH model nicely matches the behaviour of the ricepiles. (c) P(s; L) for BSD model falls as power law, until a cut off length is reached. (d) The data collapse for the BDS model nicely matches the turning-point in the behaviour of the ricepiles and the steep fall that follows, but fails to satisfactorily match their features for small s.

VIII. Conclusions

Many features of the Oslo model were qualitatively and quantitatively explained. First, it was shown the average slope tends to a constant $a_0 = 1.734 \pm 0.006$, implying the height scales linearly with lattice size for $L \gg 1$. Furthermore, the steady state height was shown following a skewed gaussian distribution, with skewness $\gamma_1 = 0.27$. Then it was proven the critical time t_c scales quadratically with size. Finally, the avalanche exponents D and τ_s were estimated for boundary and bulk-driven models, as summarised in table 7.1.

Finally, analysis of ricepiles with bigger size is encouraged to improve the obtained estimates.

References

[1] Bak P, Tang C, Wiesenfeld K. Self-Organized Criticality: An Explanation of 1/f Noise. Phys. Rev. Lett. 1987 Jul; 59(4):381-384.

[2] Watkins NW, Pruessner G, Chapman SC, et al. 25 Years of Self-organized Criticality: Concepts and Controversies. Space Sci. Rev. 2016 Jan; 198, 3–44. Available at: https://doi.org/10.1007/s11214-015-0155-x.

[3] Frette V, Christensen K, Malthe-Sørenssen A, et al. Avalanche dynamics in a pile of rice. Nature. 1996 Jan; 379, 49–52. Available at: https://doi.org/10.1038/379049a0.

[4] Christensen K, Corral A, Frette V, et al. Tracer Dispersion in a Self-Organized Critical System. Phys. Rev. Lett. 1996 Jul; 77(1), 107-110. Available at: https://link.aps.org/doi/10.1103/PhysRevLett.77.107.

[5] Christensen K, Maloney N. Complexity and Criticality. London: Imperial College Press; 2005.

[6] Pruessner G. Studies in Self-Organised Criticality. Imperial College London. 2004 Feb. Available at: https://www.ma.imperial.ac.uk/~pruess/publications/thesis_final/thesis_book.pdf.

[7] Christensen K. Complexity and Networks Course 2021-2022: Complexity Project Notes. Imperial College London. 2022 Jan. Page 4.

[8] The SciPy Community. SciPy 1.8.0. API Reference: scipy.stats.skew. Available at: https://docs.scipy.org/doc/scipy/reference/generated/scipy.stats.skew.html.

[9] Christensen K. Complexity and Networks Course 2021-2022: Complexity & Networks Social Q & A. Imperial College London. 2022 Jan. Page 6.

[10] Zhang S. On the universality of a one-dimensional model of a rice pile. Phys. Lett. 1997 Sep; 233(4-6), 317-322. Available at: https://doi.org/10.1016/S0375-9601(97)00478-7.